LASER
& PHOTONICS
REVIEWS

Laser Photonics Rev. **10,** No. 5, 791–798 (2016) / **DOI** 10.1002/lpor.201500328

Abstract High efficiency, broad bandwidth, and robust angular tolerance are key considerations in photonic device design. Here, a few-layer, asymmetric light transmitting metasurface that simultaneously satisfies all the above requirements is reported. The metasurface consists of coupled metallic sheets. It has a measured transmission efficiency of 80%, extinction ratio of 13.8 dB around 1.5 μm, and a full width half maximum bandwidth of 1.7 μm. It is as thin as 290 nm, has good performance tolerance against the angle of incidence and constituent nano-structure geometry variations. This work demonstrates a practical asymmetric light transmission device with optimal performance for large scale manufacturing.

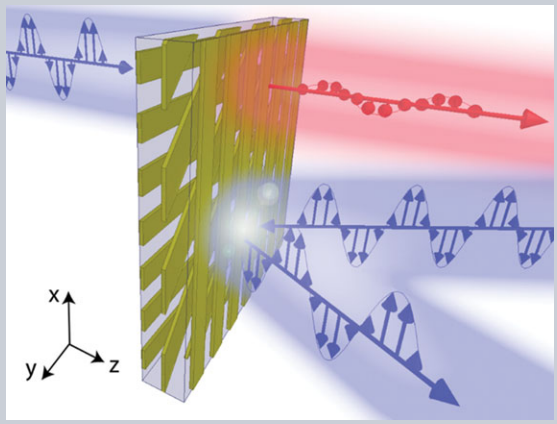

ORIGINAL
PAPER

Breaking Malus' law: Highly efficient, broadband, and angular robust asymmetric light transmitting metasurface

Cheng Zhang[1], Carl Pfeiffer[1], Taehee Jang[1], Vishva Ray[2], Maxwell Junda[3], Prakash Uprety[3], Nikolas Podraza[3], Anthony Grbic[1], and L. Jay Guo[1,*]

1. Introduction

Devices providing asymmetric transmission of light are useful components for optical communication systems, information processing, and laser applications [1–4]. Recently, asymmetric light transmission with metamaterials has received considerable interest [5–8]. Although these devices are usually reciprocal and not suitable for applications such as optical isolation [9, 10], they have unique advantages of passive operation and compact size. They can be realized using photonic crystals [11, 12], helical wires [13], hyperbolic metamaterials [14], coupled nano-antennas [15–17], and non-symmetric gratings [18, 19]. However, these devices typically suffer from complex fabrication processes, low efficiency, and limited operational bandwidth. For example, helical wires provide efficient and broadband asymmetric transmission for circularly polarized light in the infrared region [13], but they are fabricated by direct laser writing and gold plating, which is complex and time-consuming. Hyperbolic metamaterials sandwiched between two Chromium (Cr) gratings have shown broadband asymmetric light transmission as well, but exhibited a low transmission efficiency [14]. By properly designing the coupling between nano-antennas, researchers have demonstrated asymmetric light transmission [15–17]. However these structures usually require complex fabrication procedures and precise alignment between the antennas, and their efficiencies need to be further improved. A device consisting of a metallic grating cascaded with a dielectric grating provides close to 100% transmission efficiency in simulation, but has a limited bandwidth [20]. Besides, the performance of these metamaterials is usually sensitive to fabrication errors and the angle of incident light, which limits their practical applications. Further, it is also difficult to employ the same design strategy for asymmetric light transmission at different wavelength ranges.

In this work, we report on a few-layer metasurface offering efficient and broadband asymmetric transmission of light. Metasurfaces are sub-wavelength textured surfaces that can be thought of as the two-dimensional equivalent of metamaterials [21–26]. They exhibit versatile, tailored electromagnetic functions such as frequency selectivity [27, 28], polarization control [29–33], wavefront engineering [34–38], and even nonlinear responses [39–41]. The asymmetric light transmitting metasurface in this work consists of three closely-spaced layers of one-dimensional gold nano-gratings. Contrary to the prediction of conventional theory (e.g., Malus' law), the proper cascade of three layers of nano-gratings instead offers efficient and broadband asymmetric light transmission for linearly polarized light. Furthermore, the device is only 290 nm (λ/5) thick, and its performance is robust against the angle of incidence

[1] Department of Electrical Engineering and Computer Science, University of Michigan, Ann Arbor, Michigan 48109, USA
[2] Lurie Nanofabrication Facility, Department of Electrical Engineering and Computer Science, University of Michigan, Ann Arbor, Michigan 48109, USA
[3] Department of Physics and Astronomy & Wright Center for Photovoltaics Innovation and Commercialization, University of Toledo, Ohio, 43606, USA
*Corresponding author: e-mail: guo@umich.edu

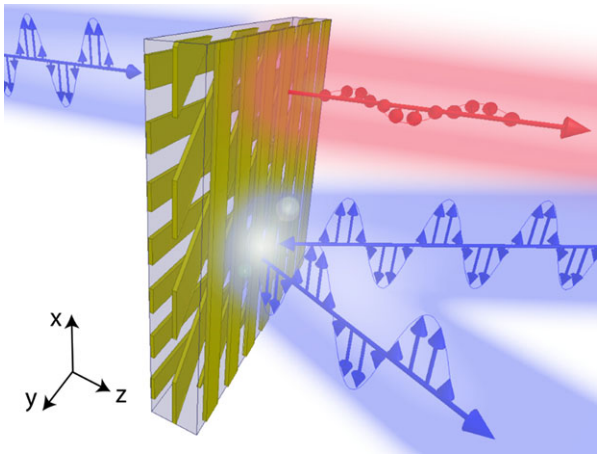

Figure 1 Artistic rendering of the metasurface, consisting of three layers of cascaded Au nano-gratings. The metasurface provides high transmission of x-polarized light incident from the left side, but blocks x-polarized light that is incident from the right side.

and fabrication variations. As an experimental demonstration, a device providing asymmetric transmission at a central wavelength of 1.5 μm is fabricated and characterized, which shows a transmission efficiency of 80%, extinction ratio of 24:1, and a full width half maximum (FWHM) operational bandwidth of 1.7 μm. Furthermore, the design concept is suitable for large-area device manufacturing and can be easily transitioned to achieve asymmetric light transmission at other wavelengths.

2. Experimental Section

The designed asymmetric light transmission metasurface consists of three layers of 40 nm thick gold (Au) nano-gratings, each of which are separated by a 125 nm thick SU-8 dielectric spacer (Fig. 1). The nano-gratings on the left and right layers have a period of 140 nm and linewidth of 70 nm. The nano-grating on the middle layer has a period of 200 nm and linewidth of 100 nm. The gratings are oriented 0°, 45°, and 90°, for the first, second, and third layers, respectively.

The metasurface was fabricated on a 500 μm thick fused silica substrate using the process shown in Fig. 2a. The bottom layer is fabricated by electron beam (E-beam) lithography (JEOL 6300FS, JEOL) using Poly(methyl methacrylate) resist (PMMA 950k, A2, Microchem) followed by the deposition of a 3 nm Titanium (Ti) adhesion layer and a 37 nm Gold (Au) layer, and then metal lift-off in an acetone solution. The PMMA layer was spin-coated on the substrate at a rate of 1600 rpm for 40 seconds, and the sample was subsequently baked on the hotplate at 180°C for 3 minutes. The PMMA thickness was about 100 nm. To solve the charging issues during the E-beam writing, a conductive polymer layer (E-spacer, SHOWA DENKO K.K. 13–9, Shiba Daimon 1-Chome Minato-Ku, Japan) was spin-coated onto the PMMA layer at a rate of 1500 rpm for 45 seconds, and the sample was subsequently baked on the hotplate at 110°C for 2 minutes. The E-spacer layer thickness was about 20 nm. After the E-beam writing, the E-spacer layer was removed after the sample was rinsed in the DI water for 15 seconds. Subsequently, the PMMA layer was developed in the developer solution (1:3 MIBK to IPA) for 45 seconds, and rinsed in IPA for another 30 seconds. To achieve uniform pattern features, proximity effect correction (PEC) was implemented during the E-beam writing. After the metal lift-off, a 125 nm thick SU-8 layer was spun on the metal layer and cured with ultraviolet (UV) radiation (MJB2, Karl Suss). The patterning and metal deposition / lift-off process was repeated three times in order to fabricate all three layers. The scanning electron micrographs (SEMs) of the layers are shown in Figs. 2b to 2d.

The metasurface is experimentally characterized after fabrication. Output from a tunable laser (TLB 6326, Newport, central wavelength at 1.5 μm) was sent through a polarization controller (FPC032, Thorlabs), a single mode optical fiber (P3-1550A-FC-1, Thorlabs), and then onto the metasurface. The polarization state from the input fiber was adjusted by the polarization controller and confirmed by a separate linear polarizer (LPNIRA050-MP2, Thorlabs) before illuminating the metasurface. The light transmitted by the metasurface passed through another linear polarizer (LPNIRA050-MP2, Thorlabs) and was collected by an objective lens into an optical power meter (2835-C, Newport). The laser wavelength was scanned between 1470 nm and 1530 nm.

3. Results

When x-polarized light is incident from the left side, it is efficiently transmitted through the metasurface and converted to y-polarized output. In contrast, there is very little transmission of x-polarized light when incident from the right (opposite) side of the metasurface. Therefore, this metasurface provides asymmetric transmission for linearly polarized light.

Each layer of the Au nano-gratings individually functions as a linear polarizer, which transmits light polarized orthogonal to the grating, while absorbing/reflecting light polarized along the grating. According to Malus' law, the transmission intensity of a linearly polarized light through a linear polarizer is: $I = I_0\cos^2\theta$, where I_0 and I are the light intensity before and after the polarizer, and θ is the angle between the incident light polarization direction and the polarizer transmission axis. In an ideal case where the metallic nano-gratings provide unity light transmission, there will only be 25% transmission intensity for x-polarized light incident from the left side through the cascaded system of three linear polarizers whose transmission axes are rotated 45° with respect to each other. When the finite cell size and material absorption are taken into account, the efficiency is even lower. Figure S1 (Supporting Information) plots the product of the Jones matrices for the 3 different layers, which is based on Malus' law and neglects multiple reflections between the layers. The notation T_{nm} means

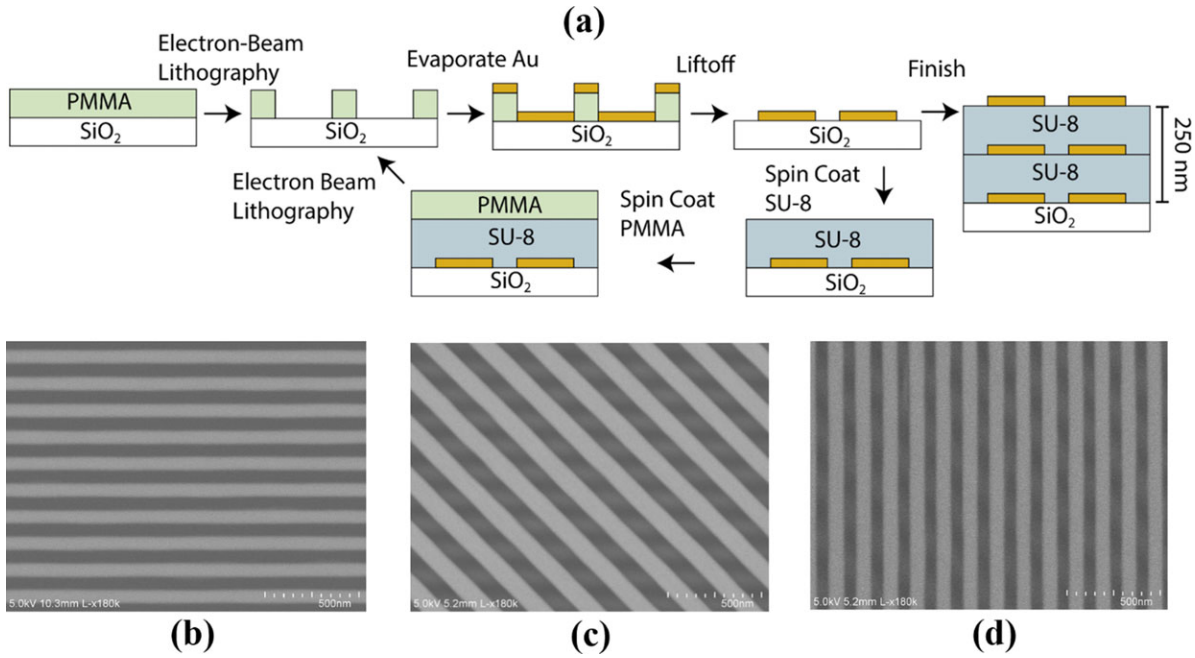

Figure 2 (a) Metasurface fabrication flow chart; (b-d) SEM pictures of the bottom (b), middle (c) and top (d) layer.

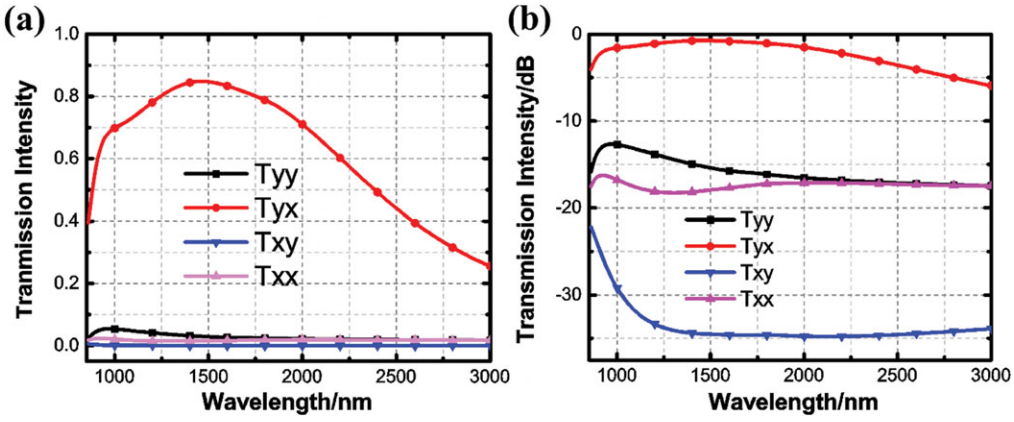

Figure 3 Simulated transmission intensity through the metasurface in linear (a) and logarithmic (b) scale.

transmission intensity of *m-polarized* input light into *n-polarized* output light.

However, Malus' law breaks down for the proposed structure consisting of closely spaced Au gratings. Next, the three layers of cascaded Au nano-gratings are treated as an integrated structure and its electromagnetic response is calculated (linear scale in Fig. 3a and logarithmic scale in Fig. 3b, see Supporting Information for additional details). In contrast to the predictions of Malus' law, this metasurface provides high transmission of x-polarized light when it is incident from the left side, while blocking the same polarization incident from the right side. The simulated transmission efficiency around 1.5 μm is 85% with an extinction ratio of 53 (17.2 dB). The extinction ratio is defined as the ratio of the transmittance of x-polarized light from the left side ($T_{yx} + T_{xx}$) to the transmittance of x-polarized light from the right side ($T_{xy} + T_{xx}$). The device has a FWHM operating bandwidth of 1.67 μm. Malus' law only applies to cases where the multiple reflections between layers are negligible. However, for the metasurface here, there are strong multiple reflections between the Au nano-grating layers. Such interaction leads to asymmetric light transmission as well as polarization conversion in the structure.

The asymmetric response is due to a "cavity effect" rather than the near field coupling between layers. The multiple reflections between the three layers in the three-layer metasurface leads to an enhanced cross-polarization transmittance (T_{yx}) over a broad bandwidth, as well as suppressed transmittances of other co- and cross-polarization conversions (T_{yy}, T_{xy}, and T_{xx}). This results in the asymmetric light transmission behavior of the metasurface. To better illustrate this point, we extracted the effective anisotropic impedance of each grating layer first, and then replaced the metasurface with three infinitesimally

thin sheets which have the extracted impedances of the grating layers. Such a modelling process takes into account the "cavity effect". As shown in Fig. S2, the simulated transmittance of the three "equivalent sheets" corresponds well with the simulated transmittance of the actual metasurface.

Cascading two orthogonal 1D metallic gratings (e.g., bottom and top grating layers in Fig. 1) will lead to weak co-polarization conversions, and negligible cross-polarization conversions. There will also be some weak "cavity effect" in this two-layer structure depending on the separation between the layers, as shown in Fig. S3. However, the 45° orientated middle grating works as an efficient polarization conversion layer to generate cross-polarization transmission. Furthermore, such a conversion mechanism is enhanced by the cavity effect within the metasurface, which leads to its broadband asymmetric light transmission behavior.

Indeed, generating asymmetric transmission for a linear polarization requires anisotropic electric and bianisotropic responses (i.e., magneto-electric coupling). An arbitrary electric response can be generated using a single layer patterned sheet. However, a single sheet cannot generate magnetic and magneto-electric responses, which are necessary for a high-efficiency polarization conversion. In fact, the fundamental limit for cross-polarization conversion is 25% if only an electric response is utilized [42]. Therefore, we turn our attention to designs consisting of multiple layers. A systematic design method for realizing arbitrary polarization conversion is outlined in Ref. [32]. It is shown that each sheet can be homogenized as an equivalent sheet impedance with well-defined transmission and reflection coefficients. This allows the overall response of multiple cascaded sheets to be calculated, which simplifies the design procedure. It can be shown that at least 3 sheets are required to independently control electric and magnetic responses [43].

Rather than designing complicated patterns that closely approach the ideal sheets, here we show that a simplified design employing 1D metallic gratings can also achieve a relatively high performance. Consider two half-spaces separated by the metasurface, where the electric fields on either side of the metasurface are related by the following relation:

$$\begin{pmatrix} E_t^x \\ E_t^y \end{pmatrix} = \begin{pmatrix} t_{xx} & t_{xy} \\ t_{yx} & t_{yy} \end{pmatrix} \begin{pmatrix} E_i^x \\ E_i^y \end{pmatrix} = T \begin{pmatrix} E_i^x \\ E_i^y \end{pmatrix}$$

Here, T is the Jones matrix of the metasurface, and $E_i^{x/y}$ and $E_t^{x/y}$ are the incident and transmitted electric field polarized along the x and y directions, respectively. The element t_{nm} in the Jones matrix denotes transmission coefficient of the *m-polarized* electric field to the *n-polarized* electric field, and is usually a complex number (containing both field transmission amplitude and phase information). The transmission intensity coefficient T_{nm} equals the square of $|t_{nm}|$. The Jones matrix of an ideal, asymmetric transmitting device for linearly polarized light, that allows unity conversion of x-polarized light to y-polarized light, is $\mathrm{T} = e^{-i\emptyset}\left(\begin{smallmatrix} 0 & 0 \\ 1 & 0 \end{smallmatrix}\right)$ [44]. The Jones matrix of the metasurface in this study at 1.5 μm is calculated as $\left(\begin{smallmatrix} 0.126e^{i75.1^\circ} & 0.018e^{-i131^\circ} \\ 0.920e^{-i44.6^\circ} & 0.169e^{i51.9^\circ} \end{smallmatrix}\right)$, which approaches the ideal case. It has been recently demonstrated that by designing each layer with complex geometries, the metasurface performance can be further optimized [29, 32]. However, the design here, with only three layers of nano-gratings, is advantageous due to its simplicity and suitability for large area device fabrication, with a very minimal compromise of its performance.

The measured and simulated transmittance is plotted in Figs. 4a (linear scale) and 4b (logarithmic scale), showing close correspondence. The metasurface has an averaged transmission efficiency of 80% around 1.5 μm, and an extinction ratio of 24 (13.8 dB). Due to the limited output wavelength range from the laser, the device is only characterized over a narrow band. However, numerical simulation predicts its broad operational bandwidth (FWHM bandwidth of 1.7 μm). To demonstrate this, the metasurface is also characterized using a different experimental setup consisting of a rotating analyzer spectroscopic ellipsometer (Model V-VASE, J.A. Woollam Co., Inc.) between 1200 nm and 1850 nm. The illumination beam size from the ellipsometer (about 700 μm in diameter) is much larger than the metasurface area (250 μm by 250 μm square), and the measured Jones Matrix represents a superposition of the fraction of the light beam sampling the device and the surrounding area. However, since the cross-polarization conversion only takes place within the metasurface, the T_{xy} and T_{yx} components can be obtained. Figure 5 plots the simulated and measured T_{xy} and T_{yx} components. As the contributions from the device and surrounding area are not separated, the experimental values in Fig. 5 are normalized to the simulation result at 1610 nm and are in arbitrary units. The measurement demonstrates that the device behavior corresponds well with simulation over a large bandwidth. It should be noted that, due to the absorption in a fiber optic cable on the source side of the ellipsometer, there is insufficient light intensity near 1400 nm, causing the gap in the data seen there. More accurate measurements could be ascertained by using a smaller beam spot or a series of measurements of different size beam spots to appropriately quantify the Jones matrix elements for the device area only.

A visual demonstration that highlights the performance of the metasurface is shown in Figs. 4c and 4d. Figure 4c is a picture of the metasurface taken with an infrared camera when a 1.5 μm laser beam illuminates the back of the metasurface. Figure 4d corresponds to the same setup but with the metasurface flipped around so that the laser beam illuminates from the opposite side. The same laser beam intensity and polarization are maintained in the two cases. The metasurface provides high and low transmission in Figs. 4c and 4d, respectively.

4. Discussion

For many practical applications, the device performance should be robust to the variations in the angle of incidence [27]. This also helps reduce the requirements of

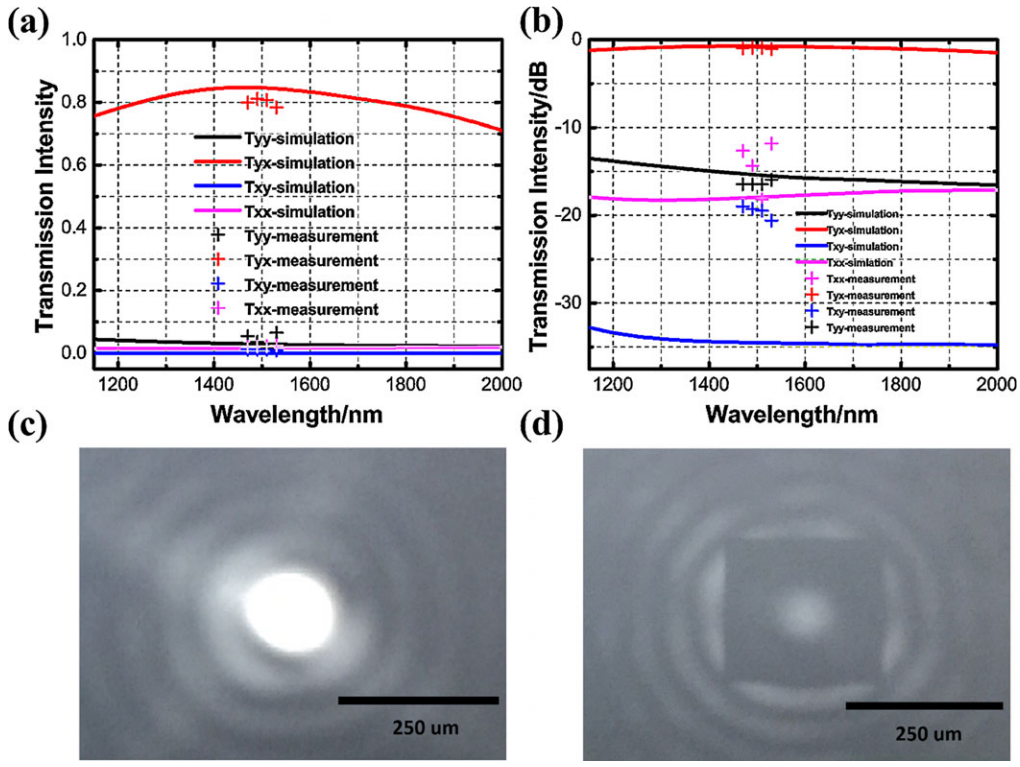

Figure 4 (a-b) Measured transmission intensity from the metasurface in linear (a) and logarithmic (b) scale; (c) Bright transmitted light pattern from one direction; (d) Blocked transmitted light pattern from the reverse direction. The incident laser beam intensity is kept the same in two cases.

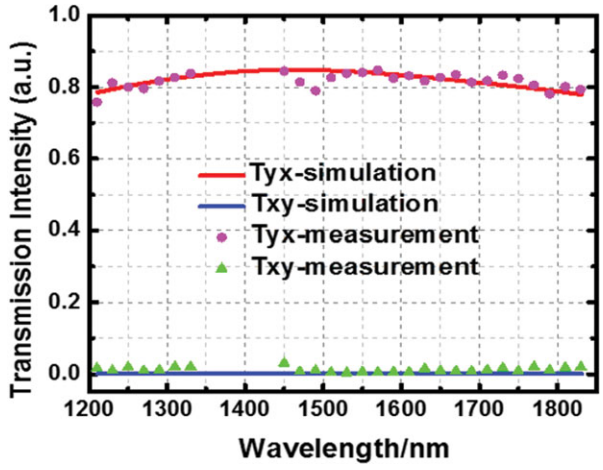

Figure 5 Measured T_{xy} and T_{yx} components with a broadband ellipsometer and large beam size. The measurement demonstrates that the device broadband behavior corresponds well with simulation.

other optical components in the system. Figures 6a and 6b plot the simulated transmittance of the metasurface at 1.5 μm versus different angles of incidence in the XZ and YZ plane. There is minimal performance degradation until the incident angle reaches 50°. As an experimental verification, the transmittance was measured at a 30° input angle (XZ and YZ plane respectively). To measure the transmission at a 30° angle of incidence, the metasurface was tilted at 30° with respect to the input single mode fiber, and the other components in the measurement set-up were kept the same. The measurement result is plotted in Figs. 6c and 6d. It can be seen that at such an incident angle, the metasurface still maintains its properties of high transmission, broad bandwidth, and good extinction ratio. The device's robust angular tolerance can be understood by examining the angular response of individual layers. Figure S4 plots the optical field reflection/transmission amplitude and phase coefficients of a single nano-grating layer at normal incidence and 30° angle incidence (in both XZ and YZ planes). It can be seen that the response from a single layer has a good angular tolerance and this contributes to the device's performance robustness against the angle of incidence.

The metasurface performance is also insensitive to variations in the grating height, width, and period. Increasing or decreasing the grating width by 20 nm does not degrade its performance (Fig. S6 in Supporting Information). Similarly, varying the grating height (from 30 nm to 60 nm) will not affect the device performance either (Fig. S7 in the Supporting Information). Every individual layer functions as a linear polarizer (anisotropic element), and its anisotropic response will not change significantly with grating width variations over a certain range (Fig. S5 in the Supporting Information). In other words, these three layers of cascaded

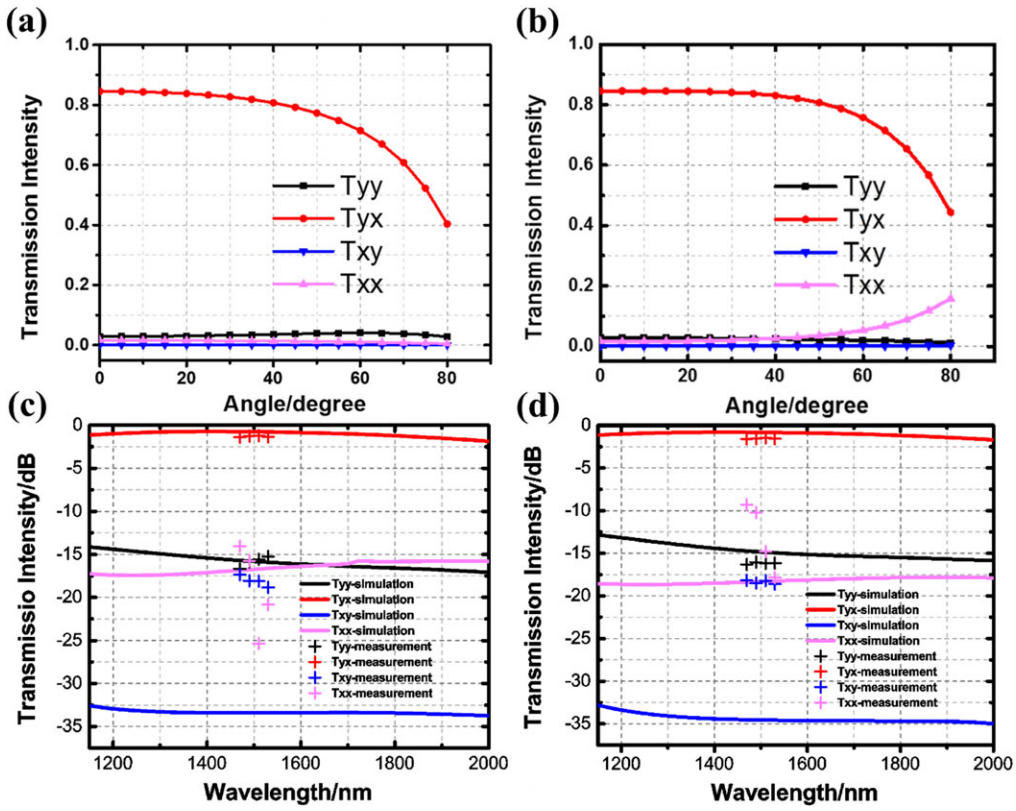

Figure 6 (a-b) Simulated transmittance at a wavelength of 1.5 μm with input light angle in the XZ (a) and YZ (b) plane; (c-d) Measured transmittance with 30 degree incident light angle in the XZ (c) and YZ (d) plane.

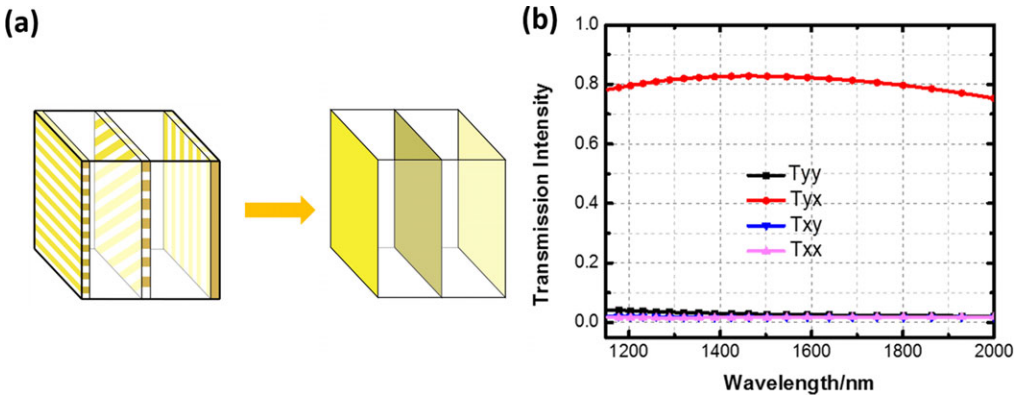

Figure 7 (a) Generalized model of the metasurface as coupled metallic sheets; (b) Simulated transmittance of metasurface with three layers of identical Au nano-gratings.

Au nano-gratings can be generalized as three layers of coupled anisotropic metallic sheets (Fig. 7a). This response also suggests that the nano-grating period can be modified without sacrificing device performance. As shown in Fig. 7b, the transmittance of the metasurface consisting of three identical layers of 40 nm thick, 70 nm wide, and 140 nm period Au nano-gratings is plotted, and is very similar to that of three layers of Au nano-gratings with a unique middle layer grating period in Fig. 4a (calculation details in the Supporting Information). Such a relaxation of the requirements on grating geometries (e.g., width and period) paves the way to realize large-area device fabrication for practical applications. It is true that sub-wavelength structures are usually fabricated through electron beam lithography, which is time consuming and makes it difficult to achieve large-area devices. However, for certain structures such as the nano-gratings in this study, they can be easily manufactured by various methods such as interference lithography [45], plasmonic lithography [46, 47], or nano-imprinting [48, 49]. The insensitivities of the device performance to variations in the grating geometry leave room for reasonable fabrication errors/inaccuracies.

Further, the design strategy for the metasurface can be easily extended to other wavelength ranges to achieve asymmetric light transmission devices. One simple way is to modify the spacer layer thickness. As shown in Fig. S8 in the Supporting Information, asymmetric light transmission centered at 1 μm and 2 μm can be realized by setting the spacer thickness as 70 nm and 260 nm respectively. Moving the current design employing Gold to the visible regime will lead to a performance degradation, because of the high optical loss associated with Gold in this wavelength range. Improved designs can be achieved by selecting lower loss constituent materials (e.g., Silver or Aluminum) [50], and adjusting the geometry of the constituent layers in order to achieve impedance matching with air to suppress the reflections.

5. Conclusions and Outlook

In summary, a thin (λ/5) asymmetric light transmitting metasurface is designed and experimentally demonstrated. It has the advantages of high transmission (80%), broad bandwidth (FWHM bandwidth of 1.7 μm), and good extinction ratio (24; 13.8 dB). In addition, its performance is insensitive to both the incident light angle and the constituent nano-structure geometric variations. A comparison between the metasurface in this work and recently reported structures is listed in Table S1 in the Supporting Information, where the metasurface in this study shows a comparable or better performance in terms of the bandwidth, efficiency, and foot print. Furthermore, the design principle is general and can be applied to other wavelength ranges. In addition, the device structure is suitable for large-area device manufacturing techniques such as a nano-imprinting or roll-to-roll printing.

Supporting Information

Additional supporting information may be found in the online version of this article at the publisher's website.

Acknowledgements. This work is supported by the NSF Materials Research Science and Engineering Center (MRSEC) program DMR 1120923. The authors acknowledge the technical support from the Lurie Nanofabrication Facility (LNF) at the University of Michigan. C. Zhang acknowledges the discussions with Dr. Young Jae Shin, Dr. Tao Ling, and Mr. Chengang Ji. M. Junda, P. Uprety, and N. Podraza acknowledge the support by the Ohio Department of Development (ODOD) Ohio Research Scholar Program (Northwest Ohio Innovators in Thin Film Photovoltaics, Grant No. TECH 09-025).

Received: 23 December 2015, **Revised:** 29 June 2016, **Accepted:** 4 July 2016

Published online: 12 August 2016

Key words: asymmetric light transmission, metasurface, metamaterial, angle-insensitive device, plasmonics.

References

[1] J. Y. Chin, T. Steinle, T. Wehlus, D. Dregely, T. Weiss, V. I. Belotelov, et al., Nat. Commun. **4**, 1599 (2013).
[2] J. L. O'Brien, G. J. Pryde, A. G. White, T. C. Ralph, and D. Branning, Nature **426**, 264–267 (2003).
[3] E. Knill, R. Laflamme, and G. J. Milburn, Nature **409**, 46–52 (2001).
[4] R. Fleury, D. L. Sounas, C. F. Sieck, M. R. Haberman, and A. Alù, Science **343**, 516–519 (2014).
[5] R. Singh, E. Plum, C. Menzel, C. Rockstuhl, A. K. Azad, R. A. Cheville, et al., Phys. Rev. B **80**, 153104, 2009).
[6] S. Cakmakyapan, A. E. Serebryannikov, H. Caglayan, and E. Ozbay, Opt. Express **20**, 26636–26648 (2012).
[7] C. Menzel, C. Helgert, C. Rockstuhl, E. B. Kley, A. Tünnermann, T. Pertsch, et al., Phys. Rev. Lett. **104**, 253902 (2010).
[8] V. A. Fedotov, A. S. Schwanecke, N. I. Zheludev, V. V. Khardikov, and S. L. Prosvirnin, Nano Lett. **7**, 1996–1999 (2007).
[9] D. Jalas, A. Petrov, M. Eich, W. Freude, S. Fan, Z. Yu, et al., Nat. Photonics **7**, 579–582 (2013).
[10] L. Bi, J. Hu, P. Jiang, D. H. Kim, G. F. Dionne, L. C. Kimerling, et al., Nat. Photonics **5**, 758–762 (2011).
[11] A. Cicek, M. B. Yucel, O. A. Kaya, and B. Ulug, Opt. Lett. **37**, 2937–2939 (2012).
[12] C. Wang, X.-L. Zhong, and Z.-Y. Li, Sci. Rep. **2** (2012).
[13] J. K. Gansel, M. Thiel, M. S. Rill, M. Decker, K. Bade, V. Saile, et al., Science **325**, 1513–1515 (2009).
[14] T. Xu and H. J. Lezec, Nat. Commun. **5** (2014).
[15] S. Wu, S. Xu, Y. Zhang, Y. Wu, J. Jiang, Q. Wang, et al., Opt. Lett. **39**, 6426–6429 (2014).
[16] F. Qin, L. Ding, L. Zhang, F. Monticone, C. C. Chum, J. Deng, et al., Sci. Adv. **2** (2016).
[17] Z. Li, S. Chen, C. Tang, W. Liu, H. Cheng, Z. Liu, et al., Appl. Phys. Lett. **105**, 201103 (2014).
[18] S. Cakmakyapan, H. Caglayan, A. E. Serebryannikov, and E. Ozbay, Appl. Phys. Lett. **98**, 051103 (2011).
[19] S. Cakmakyapan, A. E. Serebryannikov, H. Caglayan, and E. Ozbay, Opt. Lett. **35**, 2597–2599 (2010).
[20] Z. H. Zhu, K. Liu, W. Xu, Z. Luo, C. C. Guo, B. Yang, et al., Opt. Lett. **37**, 4008–4010 (2012).
[21] A. E. Minovich, A. E. Miroshnichenko, A. Y. Bykov, T. V. Murzina, D. N. Neshev, and Y. S. Kivshar, Laser Photonics Rev. **9**, 195–213 (2015).
[22] N. Yu and F. Capasso, Nat. Mater. **13**, 139–150 (2014).
[23] Y. Nanfang, P. Genevet, F. Aieta, M. A. Kats, R. Blanchard, G. Aoust, et al., IEEE J. Sel. Top. Quant. Electr. **19**, 4700423–4700423 (2013).
[24] A. V. Kildishev, A. Boltasseva, and V. M. Shalaev, Science **339**, (2013).
[25] C. Pfeiffer and A. Grbic, Phys. Rev. Lett. **110**, 197401 (2013).
[26] H. Cheng, Z. Liu, S. Chen, and J. Tian, Adv. Mater., 5410–5421 (2015).
[27] Y.-K. R. Wu, A. E. Hollowell, C. Zhang, and L. J. Guo, Sci. Rep. **3** (2013).
[28] A. Shaltout, J. Liu, V. M. Shalaev, and A. V. Kildishev, Nano Lett. **14**, 4426–4431 (2014).

[29] C. Pfeiffer, C. Zhang, V. Ray, L. J. Guo, and A. Grbic, Phys. Rev. Lett. **113**, 023902 (2014).
[30] Y. Yang, W. Wang, P. Moitra, I. I. Kravchenko, D. P. Briggs, and J. Valentine, Nano Lett. **14**, 1394–1399 (2014).
[31] N. K. Grady, J. E. Heyes, D. R. Chowdhury, Y. Zeng, M. T. Reiten, A. K. Azad, et al., Science **340**, 1304–1307 (2013).
[32] C. Pfeiffer and A. Grbic, Phys. Rev. Appl. **2**, 044011 (2014).
[33] C. Pfeiffer, C. Zhang, V. Ray, L. Jay Guo, and A. Grbic, Optica **3**, 427–432 (2016).
[34] D. Lin, P. Fan, E. Hasman, and M. L. Brongersma, Science **345**, 298–302 (2014).
[35] X. Ni, S. Ishii, A. V. Kildishev, and V. M. Shalaev, Light Sci. Appl. **2**, e72 (2013).
[36] C. Pfeiffer, N. K. Emani, A. M. Shaltout, A. Boltasseva, V. M. Shalaev, and A. Grbic, Nano Lett. **14**, 2491–2497 (2014).
[37] C. Pfeiffer and A. Grbic, Phys. Rev. Appl. **2**, 044012 (2014).
[38] P. R. West, J. L. Stewart, A. V. Kildishev, V. M. Shalaev, V. V. Shkunov, F. Strohkendl, et al., Opt. Express **22**, 26212–26221 (2014).
[39] R. Czaplicki, H. Husu, R. Siikanen, J. Mäkitalo, M. Kauranen, J. Laukkanen, et al., Phys. Rev. Lett. **110**, 093902 (2013).
[40] J. A. H. van Nieuwstadt, M. Sandtke, R. H. Harmsen, F. B. Segerink, J. C. Prangsma, S. Enoch, et al., Phys. Rev. Lett. **97**, 146102 (2006).
[41] G. Li, S. Chen, N. Pholchai, B. Reineke, P. W. H. Wong, E. Y. B. Pun, et al., Nat. Mater. **14**, 607–612 (2015).
[42] F. Monticone, N. M. Estakhri, and A. Alù, Phys. Rev. Lett. **110**, 203903 (2013).
[43] C. Pfeiffer and A. Grbic, IEEE Trans. Microw. Theory Tech. **61**, 4407–4417 (2013).
[44] C. Menzel, C. Rockstuhl, and F. Lederer, Phys. Rev. A **82**, 053811 (2010).
[45] C. Lu and R. H. Lipson, Laser Photonics Rev. **4**, 568–580 (2010).
[46] X. Chen, F. Yang, C. Zhang, J. Zhou, and L. J. Guo, ACS Nano **10**, 4039–4045 (2016).
[47] W. Srituravanich, N. Fang, C. Sun, Q. Luo, and X. Zhang, Nano Lett. **4**, 1085–1088 (2004).
[48] C. Zhang, H. Subbaraman, Q. Li, Z. Pan, J. G. Ok, T. Ling, et al., J. Mater. Chem. C **4**, 5133–5153 (2016).
[49] L. J. Guo, Adv. Mater. **19**, 495–513 (2007).
[50] C. Zhang, D. Zhao, D. Gu, H. Kim, T. Ling, Y.-K. R. Wu, et al., Adv. Mater. **26**, 5696–5701 (2014).